RSC Advances

PAPER

View Article Online
View Journal | View Issue

Cite this: *RSC Adv.*, 2016, **6**, 49429

Compositional effect of Cr contamination susceptibility of $La_{9.83}Si_{6-x-y}Al_xFe_yO_{26\pm\delta}$ apatite-type SOFC electrolytes in contact with CROFER 22 APU†

P. K. Pandis,[ab] E. Xenogiannopoulou,[c] P. M. Sakkas,[b] G. Sourkouni,[de] Ch. Argirusis[be] and V. N. Stathopoulos*[a]

Received 22nd January 2016
Accepted 4th May 2016

DOI: 10.1039/c6ra02025a

www.rsc.org/advances

Apatite-type lanthanum silicates (ATLS) are attracting great interest as a new class of solid electrolytes possessing high oxide-ion conductivity at relatively low temperatures for solid oxide fuel cells (SOFC). In this study, doped ATLS of the composition $La_{9.83}Si_{6-x-y}Al_xFe_yO_{26\pm\delta}$ (x: 0, 0.25, 0.75, 1.5 and/or y: 0, 0.25, 0.75, 1.5) were successfully prepared by solid state chemistry. They were brought into direct contact with CROFER-22 interconnector alloy in order to study Cr migration into the electrolyte. Due to inconclusive SEM-EDX results, a depth profile was acquired by Laser Induced Breakdown Spectroscopy (LIBS) and the results showed that the increase of Fe concentration in the apatite oxide's composition enhanced Cr uptake. At the same time, lower conductivity values were measured for the materials after Cr contamination *i.e.* in Fe containing ATLS. No significant change in conductivity was found for Fe-free ATLS sample.

Introduction

Research effort has been attracted towards the study of apatite-type lanthanum silicates (ATLS) materials as potential electrolytes in solid oxide fuel cell (SOFC) technology mainly due to their high conductivity at moderate temperatures (600–800 °C).[1–16] However drawbacks have also been identified for silicate apatite electrolytes and their practical application. High sintering temperatures are required for the preparation of dense electrolyte layers[1,3,5,8–10] but composition can tune the refractoriness of such materials.[3,16] Generally such silicate apatites show high structural stability but electrode deposition is not straight forward.[17] Furthermore poor cell or half-cell performance is observed due to Si migration towards the electrolyte/electrode interface.[17,18] Poor electrode performance is found due to solid state reactions between ATLS and certain types of electrodes.[16–18] A review on the above advantages, drawbacks including fabrication issues and approaches towards cell and/or suitable electrodes is given by Sadykov *et al.*[16] In the design of a SOFC stack the interconnector plays a significant role in its structural and electrical behavior. It is a structural component in contact with both cathode and anode electrode of the SOFC and must be oxidation resistant, impermeable to the diffusion gases, and chemically stable. Another important function of interconnect is the separation of fuel and air as well as the electronic conduction among adjacent cells.[19–25] A variety of advanced ceramic materials have been tested, with $LaCrO_3$ as the state of art ceramic material but in recent years metallic interconnectors gained more attention due to their advanced properties and features compared to the ceramics. Metallic interconnects show lower cost of manufacturing, easier processing, higher electrical and thermal conductivity, high toughness, *etc.*[23–31] The fact that the SOFCs are tending to operate at intermediate temperatures (600–800 °C) is also enhancing the potential of high temperature oxidation resisting alloys (HTORs) as interconnectors rather than ceramics. The potential use of chromia-forming ferritic stainless steel has been investigated the past years because of the conductive nature of the formed Cr_2O_3 layer as compared to the traditional Al_2O_3 and SiO_2 insulators.[23,32] Cr ferritic steels such as CROFER 22 APU are the most widespread SOFC interconnects.[33–38] The weakness, though, of such chromia-forming ferritic stainless steel is volatility of Cr_2O_3 and $CrO_2(OH)_2$ at operating

[a]*Laboratory of Chemistry and Materials Technology, Department of Electrical Engineering, School of Technological Applications, Technological Educational Institute of Sterea Ellada, GR 34400, Psachna, Evia, Greece. E-mail: vasta@teihal.gr; vasta@teiste.gr*

[b]*School of Chemical Engineering, National Technical University of Athens, 15780 Athens, Greece*

[c]*Materials Industrial Research & Technology Center S.A., 72nd km of Athens-Lamia National Road, P.O. Box 18646, GR 34100 Chalkida, Greece*

[d]*Institut für Energieforschung und Physikalische Technologien, Clausthal University of Technology, Robert-Koch-Str. 42, 38678 Clausthal Zellerfeld, Germany*

[e]*Clausthaler Zentrum für Materialforschung (CZM), Agricola Str. 2, 38678, Clausthal Zellerfeld, Germany*

† Electronic supplementary information (ESI) available. See DOI: 10.1039/c6ra02025a

temperatures and conditions of the fuel cells. Such chromia species formed on state of art electrodes such as $La_{1-x}Sr_xMnO_3$ (LSM) or $La_{0.6}Sr_{0.4}Co_{0.2}Fe_{0.8}O_3$ (LSCF), migrate and deposit on the triple-phase boundary (TPB) in contact with the electrolyte in use causing poisoning, overall cell performance and structural changes and eventually failure.[21,39] Especially under current, chromium is mainly deposited near the TPB along the perimeter of the pores, on the surface of the yttria stabilized zirconia (8YSZ) electrolyte particles, thereby decreasing the number of active sites necessary for oxygen reduction.[39,40] CROFER 22 behavior has been thoroughly studied in contact with electrode materials.[31,35,37–44] For the case of the state of the art LSM or LSCF cathodes, it has been reported surface segregation and migration of cationic species on the surface of the cathodes from CROFER 22 APU. Cr species are accumulated at the interface of cathode/electrolyte and on the TPB leading to lower power densities and degradation of the cell operation. In order to overcome such issues, the research effort has been focused in the development of Cr-tolerant cathodic electrodes[45] but also in the application of suitable ceramic diffusion barrier coatings.[43] Similar issues of cell degradation due to Cr are recently reported also for solid oxide electrolysis cells (SOEC).[45] Thus Cr species can affect both cathode and anode cermet side of the fuel cells. It is also reported that the extent of Cr poisoning depends not only on cathode materials but also on electrolyte to be used with cathode.[39] However regarding a new group of medium range SOFC electrolytes such as ATLS no data have been reported regarding spatial distribution of Cr ions and their poisoning effect. In the present work we investigate the interaction of ATLS based electrolytes with CROFER 22 APU metallic interconnect focusing on Cr migration. The evaluation of Cr migration into the electrolyte was monitored by SEM-EDX and laser induced breakdown spectroscopy (LIBS) measurements. LIBS was applied as a far more sensitive and versatile method.[46] LIBS, besides its industrial,[47,48] environmental,[49] biological[50] and cultural heritage[51,52] applications, is a 'non-invasive' technique that can be applied *in situ* to provide a fast tool for depth profile analysis as only a few μg are ablated from the sample.[53–55] The samples needed required no preparation so it is a very useful tool as a non-destructive analysis technique. The depth profiling of LIBS have found many applications in metals, analyzing multilayer metallic coatings,[56,57] protective paint coatings of the naval sector[58] and the oxidation behavior of metal-based super alloys.[59] On the other hand, in the field of ceramics, LIBS has been mainly applied for the depth profile analysis of cultural heritage materials such as unglazed ceramics[60,61] and the discrimination between glaze and main body of attic black ceramics,[51] while on technical ceramics, the analysis of yttria stabilized zirconia ceramic layer thermal barrier coating on a super alloy substrate[62] has been reported. A thorough review with recent LIBS applications in various fields was recently published by Carter *et al.*[63] and references therein. In this study we apply LIBS on fuel cell type materials, proving its flexibility and analytical capacity in another field of technical ceramics. The aim of this study has been the evaluation of ATLS materials on Cr poisoning by Cr species directly generated by the state-of-the-art interconnect CROFER 22 APU. For this reason, CROFER 22 APU and ATLS pellets were brought in contact at temperatures 900–1100 °C for 250–1000 h. The results of LIBS, combined also with profilometric measurements showed a compositional dependence on $La_{9.83}Si_{6-x-y}Al_xFe_yO_{26\pm\delta}$ (x: 0, 0.25, 0.75, 1.5 < 1.5 and/or y: 0, 0.25, 0.75, 1.5) ATLS materials regarding their susceptibility to contamination by Cr. AC impedance results showed that Cr poisoning has a negative effect on the electrical properties of the apatite silicates studied with a trend similar to the compositional trend of their Cr susceptibility.

Experimental

Materials synthesis

The following apatites compounds: $La_{9.83}Si_{4.5}Fe_{1.5}O_{26\pm\delta}$ (LFSO), $La_{9.83}Si_5Al_{0.25}Fe_{0.75}O_{26\pm\delta}$ (LASFO-2), $La_{9.83}Si_5Al_{0.75}Fe_{0.25}O_{26\pm\delta}$ (LASFO-1) and $La_{9.83}Si_{4.5}Al_{1.5}O_{26\pm\delta}$ (LASO) were prepared by a solid state reaction route.[3] Stoichiometric quantities of La_2O_3, SiO_2, Al_2O_3 and Fe_2O_3 with purity of 99.9% have been treated at 700 °C for 2 h in order to eliminate humidity, carbonates and impurities. The mixtures were annealed twice at 1400 °C for 10 h and ball milled for 24 h. Particle size distribution was followed by laser particle size analysis using a Malvern Mastersizer 2000 (Fig. 1S†). Pellets of 11 mm diameter and 1 mm thickness were uniaxially pressed at 3 MPa and sintered at 1500 °C for 1 h. Relative density was measured with Archimedes method and crystal phase formation was followed by powder XRD diffraction.

Samples preparation and thermal treatment

CROFER 22 APU square pieces of 12 mm × 12 mm × 0.1 mm were kept in contact with the apatite pellets under constant uniaxial weight pressure using dense alumina plates (Fig. 1). These apatites-CROFER 22 APU sets were treated at 900 °C for 1000 h, at 1000 °C for 500 h and 1100 °C for 250 h in atmospheric air with heating rate of 2 K min^{-1}. After thermal treatment, the apatite pellets were diametrically cut, casted and fine polished on the cross cut surfaces for the SEM-EDX study. No particular sample preparation was required for LIBS measurements.

Characterization of tested samples

XRD diffraction analysis was performed using CuKα radiation, λ = 1.5406 Å, 2θ range from 15–75° with scan step of 0.01° per min in a Siemens D5000 diffractometer. Both the prepared

Fig. 1 Samples of CROFER 22 APU in contact with apatite pellets. Sets are kept under constant uniaxial pressure using alumina plates.

powders and the tested pellets were measured. ICDD PDF-2 Release 2000 database was used for the identification of crystal structure with support by crystal impact Match! Software followed by Rietveld refinement with FullProf Software. XRD analysis was performed on the surface of the apatites in contact with the CROFER 22 APU in order to identify any solid state reaction at the interface. The surfaces of the apatites both in contact with the CROFER 22 APU and the open ones were observed by means of Scanning Electron Microscopy (SEM) using a JEOL6380LV, and by Laser Induced Breakdown Spectroscopy (LIBS) using LIBS2500 device, by Ocean Optics. The depth of LIBS ablation was measured by profilometry (Ambios Technology XP-2). The effect of Cr poisoning on the electrical properties of ATLS samples was investigated. AC impedance spectroscopy measurements were performed on ATLS pellets after contact with CROFER 22 APU using a SP-150 Potensiostat (Biologic Science Instruments).

LIBS specifications and parameters

The laser source of LIBS was a Q-switched, Nd:YAG laser (Model: Ultra CFR, Big Sky Laser) delivering 8.5 ns pulses, at 1064 nm, with repetition rate of 15 Hz. Plasma was generated by focusing the laser beam on the sample's surface, through a 70 mm, quartz, plano-convex lens. The light emitted by plasma was then collected by a hepta furcated fiber (one-to-seven furcation) and driven into seven HR2000 Spectrometers (Ocean Optics), each equipped with a 2048-element linear CCD array. All spectrometers are triggered to acquire and read out data simultaneously, providing the emission spectrum from UV to near IR region (200–980 nm).[51] Spectra were captured and continuously saved by LIBS software, providing a quick 'depth profile' investigation.[51–53] Therefore it was necessary to calibrate the sputter rate during LIBS in order to be able to evaluate diffusion profiles. Laser pulses of 35 mJ energy were applied at the same spot of the apatite's pellets. The successive ablation of material led to the gradual penetration of laser beam from the surface to the inner bulk. Spectra were captured and continuously saved by LIBS software, providing a 'depth profile' investigation.

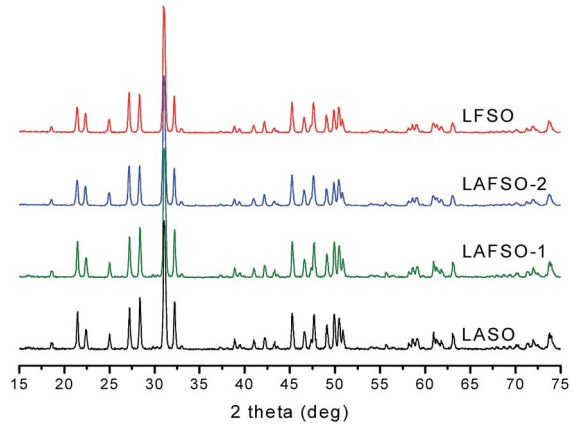

Fig. 2 XRD patterns as collected from the apatites pellets after thermal treatment at 1100 °C.

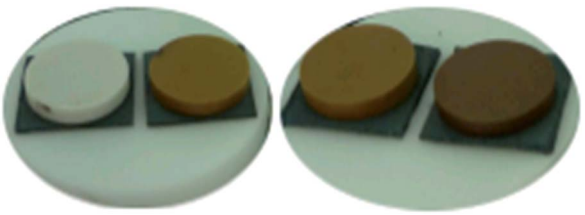

Fig. 3 Samples of LASO, LAFSO-2, LAFSO-1, LFSO (from left to right) on CROFER 22 APU, after treatment at 1000 °C for 500 h, showing no visual alterations. CROFER 22 APU supports show surface oxidation.

Table 1 Properties of the sintered ATLS samples at 1500 °C

Sample, abbreviation	Phase, space group	Relative density (%)
$La_{9.83}Si_{4.5}Fe_{1.5}O_{26\pm\delta}$, (LFSO)	Apatite, *P*36/*m* (176)	97
$La_{9.83}Si_5Al_{0.25}Fe_{0.75}O_{26\pm\delta}$, (LAFSO-2)	Apatite, *P*36/*m* (176)	97
$La_{9.83}Si_5Al_{0.75}Fe_{0.25}O_{26\pm\delta}$, (LAFSO-1)	Apatite, *P*36/*m* (176)	96
$La_{9.83}Si_{4.5}Al_{1.5}O_{26\pm\delta}$, (LASO)	Apatite, *P*36/*m* (176)	96

Results and discussion

All the prepared apatite samples (pellets) exhibited single phased crystallographic structure at the hexagonal apatite structure in space group P36/*m* (176) (PDF# 00-076-0340) (Fig. 2, 2S and 3S†).

In the end of each thermal treatment the apatite samples did not had any visual changes or findings. Nor shrinkage either color change was observed (Fig. 3). Oxidation in square CROFER 22 APU supports is clearly seen indicating significant surface formation of Cr_2O_3 layer after a typical operational time of 500 h at 1000 °C.

Properties of each sample composition after thermal treatment at 1100 °C for 250 h are depicted at Table 1. The XRD patterns after the thermal treatment at 900, 1000 and 1100 °C (Fig. 2) did not reveal any crystal phase changes or formation of any new oxides. Apatite structure is maintained in all cases with no solid state reaction identified. For example at 1100 °C the characteristic two major peaks of apatite structure at $2\theta = 31.1°$ and $2\theta = 32.2°$ showed a small shift indicating the doping effect of Al and Fe into Si site of a $La_{9.33}Si_6O_{26\pm\delta}$ apatite structure as reported elsewhere.[3,4] This small shift at major peaks was preserved even at the samples' treatment at 1100 °C indicating that no phase transition can be deduced by the interaction of apatites and CROFER 22 APU. No further shift of major peaks of the apatite spectra is found and no significant changes in the lattice parameters were observed after the thermal treatment. It may be initially concluded that no extended Cr introduction was present in the apatite structure.

This result is in good agreement with the results of McFarlane *et al.*[64] Through their systematic study of ATLS doping they concluded that no significant solubility of Cr was possible on

the ATLS phase. As reported, chromium forms $LaCrO_3$ phase due to its octahedral rather than tetrahedral coordination preference. However their approach was on a synthesis level with stoichiometric amounts of chromium.

By the SEM/EDX analysis of CROFER 22 APU specimens (Fig. 4) the visually observed surface oxidation is confirmed as a thermally grown oxide layer predominately consisting of Cr. Namely after the treatment of CROFER 22 APU at 1100 °C for 250 h, a layer of about 3 μm was created providing a Cr-rich area in-contact with apatite samples (Fig. 4). On the other hand, EDX analysis on the ATLS materials in contact with CROFER 22 APU did not clearly revealed the existence of Cr element close to the counter contact interface. In all cases the measured concentration was very low compared to the analytical method limitations and the detectability limits (<1 wt%) of the SEM/EDX unit in use. Furthermore the close positioning of Cr (L) and O (K) peak as well as the lack of Cr (K) peak limited the quantification process towards clear results on Cr content (Fig. 4S–7S and Table 1S†). No Cr was identified on the side not in contact with CROFER 22 APU in all ATLS samples. Thus, LIBS was applied in order to overcome the analytical issue named above and also to investigate its application potential as a more sensitive analytical method. From the earliest studies sensitivity of LIBS when testing solids, was reported in the ppm range with precision <10%, depending of course on various factors.[65,66]

LIBS laser pulses profilometry measurements revealed a variation in the mean ablation depth per LIBS pulse among samples (Fig. 5). After 30 pulses LASO proved its higher resistance to the mean ablation depth per pulse reaching at 32 μm while LAFSO-1 reached 43 μm, LAFOS-2 reached 51 μm and LFSO 60 μm. A clear trend in DpP with increasing Fe content is observed. This can be attributed to the refractoriness decrease of ATLS caused by Fe content.[67] This observation is in good agreement with Cowpe *et al.*[68] study that reported a relationship between sample hardness and LIBS plasma properties. Fig. 6 shows typical LIBS spectra of LAFSO-2 pellet, in the 355–368 nm spectral window.

In the contact side the three Cr characteristic lines are present, with descending intensity after 1, 8 and 30 laser pulses (Fig. 6 and 7). For comparison purposes the spectrum of the open side of the pellet is shown after 1 laser pulse, were the Cr lines are absent. LASO pellets do not present any Cr migration

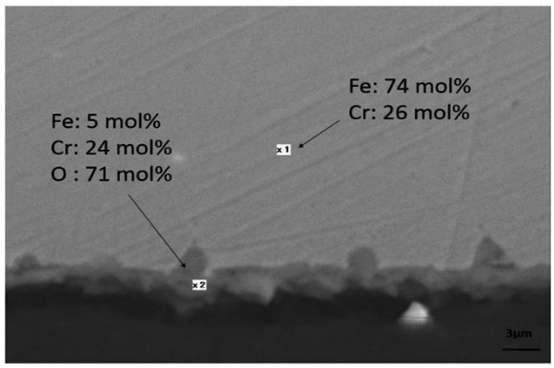

Fig. 4 CROFER 22 APU after treatment at 1100 °C for 250 h.

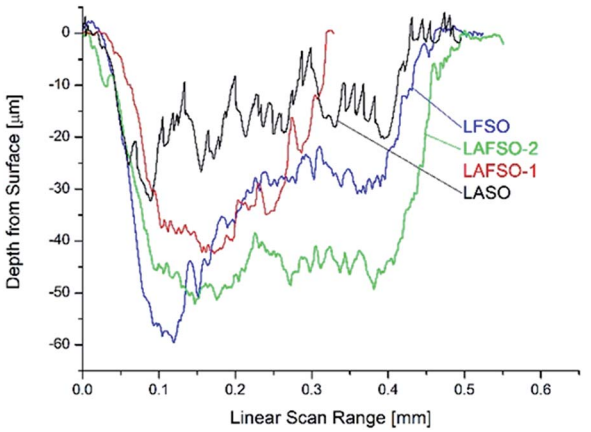

Fig. 5 Profilometry results to identify the LIBS ablation depth after 30 pulses on the side of the apatite samples in contact for 500 h at 1000 °C, with the CROFER 22 APU.

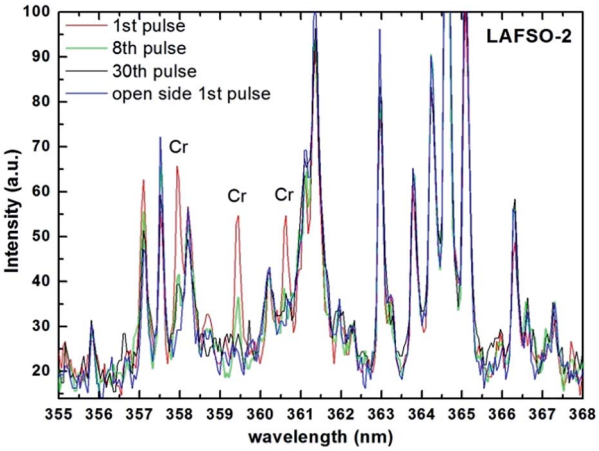

Fig. 6 Selected LIBS spectra of LAFSO-2 after 500 h at 1000 °C. Cr content at contact side after 1, 8 & 30 laser pulses and at open surface side after 1 laser pulse (laser pulse energy at 35 mJ).

into their bulk, while in the LAFSO-1 and LAFSO-2 pellets the Cr migration reaches approximately a depth of 12 μm and 15 μm respectively. The effect is more intense in the case of LFSO pellets were the Cr is still identified after 30 pulses at approximately 60 μm depth (Fig. 7). As indicated by the qualitative results of SEM/EDX, it is confirmed by LIBS that the higher is the Fe content of ATLS the easier Cr migrates into the ATLS tested. However a remarkable behavior is observed for the non Fe containing ATLS *i.e.* $La_{9.83}Si_{4.5}Al_{1.5}O_{26\pm\delta}$ LASO which is not susceptible at all in Cr migration under the tested conditions. No Cr was detected by LIBS. These are interesting results as in early ATLS synthesis studies by XRD, Cr did not show solubility in order to substitute Si in the sublattice of SiO_4 towards the formation of Cr doped apatite structure.[64] It is known that doping ATLS with Fe leads to increasing unit cell volume due to Fe^{3+} larger ionic radius compared to Al^{3+} or Si^{4+} and as the Fe content increases the structure is found hyperstoichiometric in oxygen under oxidative conditions.[67] In the same study Mossbauer measurements identified Fe^{4+} presence increasing with

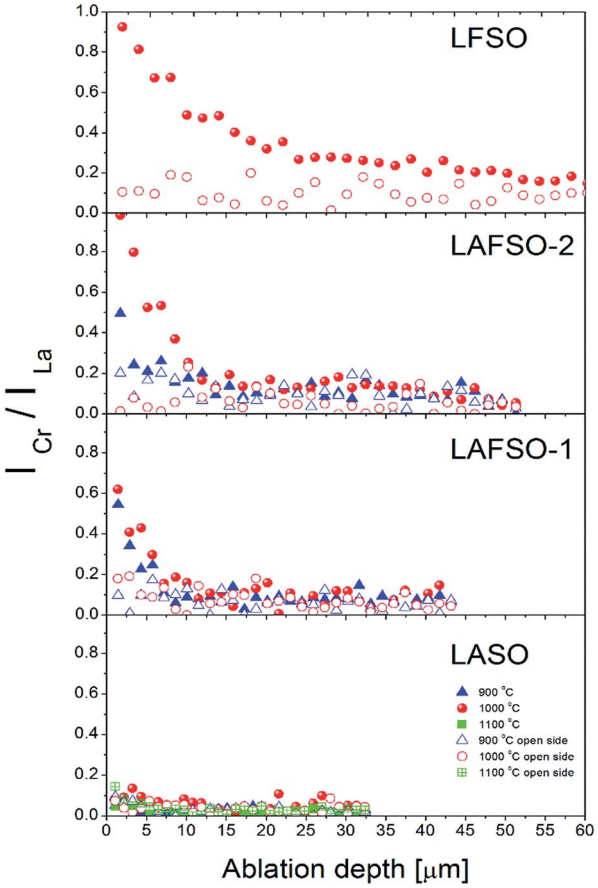

Fig. 7 LIBS results as depth profiles in 30 pulses of all the apatite pellets. The normalized peak intensity of Cr 359.349 nm characteristic line is plotted (full symbols for samples in contact with CROFER 22 APU, open symbols for open surface of samples).

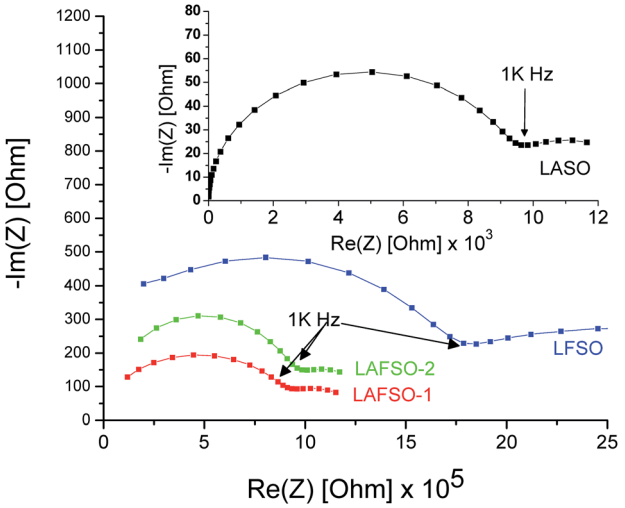

Fig. 8 Impedance plots (Nyquist) of ATLS samples obtained at 700 °C (inset: impedance spectra of LASO composition).

Table 2 Features of ATLS samples

	Particle size[a]	Sintering temperature	Conductivity at 700 °C, σ/S cm^{-1}	
Sample	d_{50}/μm	T_{SINT}/°C	This work	In ref. 3
LFSO	8.7	1500 (1 h)	5.59×10^{-7}	0.41×10^{-4}
LAFSO-2	7.5	1500 (1 h)	1.01×10^{-6}	n.a.[b]
LAFSO-1	6.5	1500 (1 h)	1.08×10^{-6}	1.07×10^{-4}
LASO	4.1	1500 (1 h)	1.05×10^{-4}	1.14×10^{-4}

[a] See ESI section. [b] n.a.: not available.

increasing total iron content in $La_{9.83}Si_{6-x-y}Al_xFe_yO_{26\pm\delta}$ caused by the A site deficiency. Similar stabilization of Fe in high oxidation states has been observed elsewhere.[69] As explained by Kharton this tendency is probably associated with a Frenkel-type disorder in O sites, induced by lanthanum vacancies.[67] As the Fe content increases lattice distortions increase and O anions displacement too towards interstitial positions. As a result La^{3+} cations as well as their vacancies are rearranged and promote stabilization of extra O into formed oxygen vacancies due to Frenkel-like disorder. However in our case the increasing tendency of Cr uptake with Fe content can be attributed to a compensation role of Cr ions on such structural distorted sites. Such an effect may have a negative impact on the conductivity properties that are strongly related to the structural disorder of ATLS structure.[67] In ATLS materials of such composition dopant's spatial distribution inhomogeneity has a strongly negative effect on oxygen mobility too.[4] Detailed studies are needed though to identify the position and coordination of Cr ions in $La_{9.83}Si_{6-x-y}Al_xFe_yO_{26\pm\delta}$ structure.

The effect of Cr poisoning on the electrical properties of apatite silicates was evaluated by impedance spectroscopy. Typical results from the LFSO, LAFSO-1, LAFSO-2 and LASO samples are shown in Fig. 8 and summarized in Table 2. The impedance spectra in all samples consist of well-defined semi-circular graphs: a large high frequency (HF) from the bulk component of the impedance and a small low frequency (LF) from grain boundary. Similar results are presented by Cao[70] and Gasparyan *et al.*[3] as far as the contributions to the overall resistance. The total conductivity of the ATLS samples tested is found lower as the Fe-content increases. Fe rich samples have also higher Cr contamination. The higher the Cr contamination is, lower total conductivity of ATLS sample is found.

In Table 2 a comparison of the conductivity values at 700 °C is made, between Cr free ATLS samples from our previous work[3] and the results on ATLS of the same composition and preparation method after being in contact with CROFER 22 APU. All Fe-containing ATLS compositions after their contact with CROFER 22 APU suffer a significant decrease in the conductivity values. LASO, on the other hand, that has no Fe in its composition and no Cr contamination shows no decrease in its conductivity. Thus Cr poisoning is significantly affecting the electrical properties of Fe containing ATLS samples.

In our previous studies the materials with the best conductivity are proven to be the Fe containing such as LFSO or LAFSO-1 and not LASO. Thus when in contact with Cr species a protective layer should be considered such as a Fe free ATLS

i.e. LASO. However in these previous studies,[3] we also report a strong influence of the synthesis and the powder processing rather than composition on conductivity properties for ATLS. Furthermore independent studies showed that $La_{9.83}Si_{4.5}Al_{1.5}O_{26.8}$ exhibits optimum conductivity.[71] From a fabrication aspect and considering the above results Fe free ATLS such as $La_{9.83}Si_{4.5}Al_{1.5}O_{26\pm\delta}$ (LASO) may be used with no constraints regarding Cr contamination. However if a Fe rich material *e.g.* LFSO, is to be used as electrolyte, a layered configuration may be designed utilizing a protective layer such as LASO type ATLS in order to prevent Cr contamination from electrode/interconnect side.

Conclusions

By SEM/EDX and LIBS analytical techniques, apatites of the $La_{9.83}Si_{6-x-y}Al_xFe_yO_{26\pm\delta}$ general formula show a clear compositional effect on their susceptibility on Cr contamination originated from CROFER 22 APU. By SEM/EDX it was not possible to quantify Cr content and the results were inconclusive. On contrary LIBS due to its much lower detection limit clearly identified Cr in the $La_{9.83}Si_{6-x-y}Al_xFe_yO_{26\pm\delta}$ samples with a depth profile clearly depending on the materials composition. Profilometry was useful for evaluating the etching depth for LIBS method. The results indicated that the increase of Fe in the apatite samples seems to enhance Cr uptake. This was mainly related to the increased lattice distortions with increasing Fe^{3+} content. $La_{9.83}Si_{4.5}Al_{1.5}O_{26\pm\delta}$ LASO was found not susceptible at all in any Cr contamination under the tested conditions. At the same time AC impedance measurements showed that LASO conductivity was also not affected. In contrast the Fe rich ATLS samples resulted in significantly lower conductivity values after being in contact with CROFER 22 APU. Total conductivity values of fresh Fe rich ATLS samples can be orders of magnitude higher but suffer a drastic decrease after Cr contamination. This drastic loss shows compositional effect similar to their susceptibility on Cr contamination. The $La_{9.83}Si_{4.5}Fe_{1.5}O_{26\pm\delta}$ material with the higher level of Cr contamination showed the lowest conductivity but also the highest conductivity loss compared to a fresh non contaminated composition. For Fe free ATLS no significant change in conductivity was observed. Thus $La_{9.83}Si_{4.5}Al_{1.5}O_{26\pm\delta}$ type of materials may be suggested as advantageous ATLS electrolytes due to their chemical inertness to Cr contamination from the triple phase boundary (TPB) Cr accumulation. Alternatively such materials can be applied as a Cr blocking layer between Fe rich ATLS type electrolytes and their respective electrodes. Such a feature may simplify the housing of an ATLS based SOFC and minimize overall cell degradation issues from Cr poisoning.

Acknowledgements

Financial support by the programs Archimedes III 'Synthesis, Characterization and study of properties of solid electrolytes of the apatite structure for fuel cell applications – APACELL' implemented within the framework of Education and Lifelong Learning Operational Programme, co-financed by the Hellenic Ministry of Education, is gratefully acknowledged.

References

1 T. Kharlamova, S. Pavlova, V. A. Sadykov, Y. Bespalko, T. Krieger, O. Lapina, D. Khabibulin, V. Muzykantov, M. Chaikina, N. Uvarov, Y. Pavlukhin, V. Kriventsov, S. Petrov, C. Argirusis and V. Kaichev, *ECS Trans.*, 2009, **25**, 1791.
2 H. Gasparyan, C. Argirusis, C. Szepanski, G. Sourkouni, V. Stathopoulos, T. Kharlamova, V. A. Sadykov and S. Bebelis, *ECS Trans.*, 2009, **25**, 2681.
3 H. Gasparyan, S. Neophytides, D. Niakolas, V. Stathopoulos, T. Kharlamova, V. Sadykov, O. Van der Biest, E. Jothinathan, E. Louradour, J.-P. Joulin and S. Bebelis, *Solid State Ionics*, 2011, **192**, 158.
4 V. Sadykov, E. Sadovskaya, A. Bobin, T. Kharlamova, N. Uvarov, A. Ulikhin, C. Argirusis, G. Sourkouni and V. Stathopoulos, *Solid State Ionics*, 2015, **271**, 69.
5 T. Kharlamova, O. Vodyankina, A. Matveev, V. Stathopoulos, A. Ishchenko, D. Khabibulin and V. Sadykov, *Ceram. Int.*, 2015, **41**, 13393–13408.
6 V. Chalkia, P. Pandis and V. N. Stathopoulos, *ECS Trans.*, 2015, **68**, 2339–2348.
7 P. Pandis, T. Kharlamova, V. Sadykov and V. N. Stathopoulos, *MATEC Web Conf.*, 2016, **41**, 04001.
8 A. Shaula, V. Kharton and F. Marques, *Solid State Ionics*, 2006, **177**, 1725–1728.
9 A. L. Shaula, V. V. Kharton and F. M. B. Marques, *J. Solid State Chem.*, 2005, **178**, 2050–2061.
10 X. G. Cao and S. P. Jiang, *J. Alloys Compd.*, 2012, **523**, 127–133.
11 X. G. Cao and S. P. Jiang, *J. Mater. Chem. A*, 2014, **2**, 20739–20747.
12 S. P. Jiang, L. Zhang, H. Q. He, R. K. Yap and Y. Xiang, *J. Power Sources*, 2009, **189**, 972–981.
13 L. León-Reina, E. R. Losilla, M. Martínez-Lara, S. Bruque and M. A. G. Aranda, *J. Mater. Chem.*, 2004, **14**, 1142–1149.
14 A. Yaremchenko, A. Shaula, V. Kharton, J. C. Warenborgh, D. P. Rojas, M. V. Patrakeev and F. M. B. Marques, *Solid State Ionics*, 2004, **171**, 51–59.
15 H. Yoshioka and S. Tanase, *Solid State Ionics*, 2005, **176**, 2395–2398.
16 V. Sadykov, T. Kharlamova, S. Pavlova, V. Muzykantov, A. Ishchenko, T. Krieger, O. Lapina, N. Uvarov, M. Chaikina, Yu. Pavlyukhin, Ch. Argirusis, S. Bebelis, H. Gasparyan, V. Stathopoulos, E. Jothinathan and O. Van der Biest, *Lanthanum Compounds, Production and Applications*, Nova Science Publishers, Inc., Hauppauge, NY, 2010, pp. 1–126.
17 D. Marrero-López, M. C. Martín-Sedeño, J. Peña-Martínez, J. C. Ruiz-Morales, P. Núñez, M. A. G. Aranda and J. R. Ramos-Barrado, *J. Power Sources*, 2010, **195**, 2496–2506.
18 E. V. Tsipis and V. V. Kharton, *J. Solid State Electrochem.*, 2011, **15**, 1007–1040.
19 P. Huczkowski, N. Christiansen, V. Shemet, J. Piron-Abellan, L. Singheiser and W. J. Quadakkers, *J. Fuel Cell Sci. Technol.*, 2004, **1**, 30.
20 *Interconnects in high temperature solid oxide fuel cells*, ed. H. U. Anderson, F. Tietz, S. C. Singhal and K. Kendall, Amsterdam, Elsevier, 2003, ch. 7.

21 J. W. Fergus, *Mater. Sci. Eng., A*, 2005, **397**, 271–283.
22 W. J. Quaddakkers, J. Piron-Abellan, V. Shemet and L. Singheiser, *Mater. High Temp.*, 2003, **20**, 115.
23 Z. G. Yang, K. S. Weil, D. M. Paxton and J. W. Stevenson, *J. Electrochem. Soc.*, 2003, **150**, A1188.
24 T. A. Morris, E. A. Barrringer, S. C. Kung and R. W. McKain, *MRS Bull.*, 2005, **30**, 59.
25 W. Z. Zhu and S. C. Deevi, *Mater. Sci. Eng., A*, 2003, **227**, 348.
26 Z. G. Yang, *Int. Mater. Rev.*, 2008, **53**, 39.
27 W. J. Quadakkers, V. Shemet and L. Singheiser, *US Pat.*, no. 2,003,059,335, 2003.
28 J. P. Abeilan, V. Shemet, F. Tietz, L. Singheiser and W. J. Quadakkers, in *Proceedings of the Seventh International Symposium on Solid Oxide Fuel Cells, The Electrochemical Proceedings Series*, ed. S. C. Singhal and M. Dokiya, Pennington, NJ, PV2001-16, 2001, p. 811.
29 Z. G. Yang, J. S. Hardy, M. S. Walker, G. Xia, S. P. Simner and J. W. Stevenson, *J. Electrochem. Soc.*, 2004, **151**, A1825.
30 K. Huang, P. Y. Hou and J. B. Goodenough, *Solid State Ionics*, 2000, **129**, 237.
31 Z. Yang, G. G. Xia, X. H. Li and J. W. Stevenson, *Int. J. Hydrogen Energy*, 2007, **32**, 3648.
32 Z. Yang, G. G. Xia, S. P. Simner and J. W. Stevenson, *J. Electrochem. Soc.*, 2005, **152**, A1896.
33 M. R. Bateni, P. Wei, X. Deng and A. Petric, *Surf. Coat. Technol.*, 2007, **201**, 4677.
34 S. P. Simner, M. D. Anderson, G. G. Xia, Z. G. Yang, L. R. Pederson and J. W. Stevenson, *J. Electrochem. Soc.*, 2005, **152**, A740.
35 Y. Matsuzaki and I. Yasuda, *Solid State Ionics*, 2000, **132**, 271.
36 Y. S. Taniguchi, M. Kadowaki, H. Kawamura, T. Yasuo, Y. Akiyama and Y. Miyake, *J. Power Sources*, 1995, **55**, 73.
37 Y. Matsuzaki and I. Yasuda, *J. Electrochem. Soc.*, 2001, **148**, A126.
38 H. Yokokawa and T. Horita, *Solid Oxide Fuel Cell Materials: Durability, Reliability and Cost, Encyclopedia of Sustainability Science and Technology*, Springer Science & Business Media, New York, 2013.
39 E. Konysheva, H. Penkalla, E. Wessel, J. Mertens, U. Seeling, L. Singheiser and K. Hilpert, *J. Electrochem. Soc.*, 2006, **153**, A765.
40 Z. Yang, G. G. Xia, G. D. Maupin and J. W. Stevenson, *Surf. Coat. Technol.*, 2006, **201**, 4476.
41 I. Zhitomirsky and A. Petric, *J. Eur. Ceram. Soc.*, 2002, **20**, 2055.
42 J. Froitzheim, *Ferritic Steel Interconnectors and their Interactions with Ni Base Anodes in Solid Oxide Fuel Cells (SOFC)*, Schriften des Forschungszentrums Jülich Reihe Energie & Umwelt/Energy & Environment, 2008, p. 16.
43 J. H. Choi, T. Lee, M. Choi, Y.-S. Yoo and S.-W. Baek, *Int. J. Hydrogen Energy*, 2010, **35**, 4285.
44 S. P. Jiang and X. Chen, *Int. J. Hydrogen Energy*, 2004, **39**, 505–531.
45 K. Chen, J. Hyodo, A. Dodd, N. Ai, T. Ishihara, L. Jian and S. P. Jiang, *Faraday discuss.*, 2015, **182**, 457–476.
46 T. A. Labutin, V. N. Lednev, A. A. Ilyinc and A. M. Popov, *J. Anal. At. Spectrom.*, 2016, **16**, 90–118.
47 P. Stavropoulos, C. Palagas, G. N. Angelopoulos, D. N. Papamantellos and S. Couris, *Spectrochim. Acta, Part B*, 2004, **59**, 1885.
48 P. L. García, J. M. Vadillo and J. J. Laserna, *J. Appl. Spectrosc.*, 2004, **58**, 1347.
49 S. G. Buckley, H. A. Johnsen, K. R. Hencken and D. W. Hahn, *Waste Manag.*, 2000, **20**, 455.
50 J. D. Hybl, G. A. Lithgow and S. G. Buckley, *Appl. Spectrosc.*, 2003, **57**, 1207.
51 E. Xenogiannopoulou, C. Andreouli and C. Stournaras, *J. Nano Res.*, 2009, **8**, 61.
52 K. Melessanaki, M. Mateo, S. C. Ferrence, P. P. Betancourt and D. Anglos, *Appl. Surf. Sci.*, 2002, **156**, 197.
53 P. K. Diwakar, K. H. Loper, A.-M. Matiaske and D. W. Hahn, *J. Anal. At. Spectrom.*, 2012, **27**, 1110.
54 R. Sattmann, I. Mönch, H. Krause, R. Noll, S. Couris, A. Hatziapostolou, A. Mavromanolakis, C. Fotakis, E. Larrauri and R. Miguel, *Appl. Spectrosc.*, 1998, **52**, 456.
55 L. J. Radziemski and D. A. Cremers, *Handbook of laser-induced breakdown spectroscopy*, John Wiley, New York, 2006.
56 J. M. Vadillo and J. J. Laserna, *J. Anal. At. Spectrom.*, 1997, **12**, 859–862.
57 M. P. Mateo, J. M. Vadillo and J. J. Laserna, *J. Anal. At. Spectrom.*, 2001, **16**, 1317–1321.
58 M. P. Mateo, V. Pinon and G. Nicolas, *Surf. Coat. Technol.*, 2012, **211**, 89–92.
59 T.-H. Kim, D.-H. Lee, D. Kim, C. Jang and J.-I. Yun, *J. Anal. At. Spectrom.*, 2012, **27**, 1525–1531.
60 A. J. Lopez, G. Nicolas, M. P. Mateo, V. Pinon, M. J. Tobar and A. Ramil, *Spectrochim. Acta, Part B*, 2005, **60**, 1149–1154.
61 I. Osticioli, J. Argesti, C. Fornacelli, I. Turbani Memmi and S. Siano, *J. Anal. At. Spectrom.*, 2012, **27**, 827–833.
62 D. K. Das, J. P. McDonald, S. M. Yalisove and T. M. Pollock, *Spectrochim. Acta, Part B*, 2008, **63**, 27–36.
63 S. Carter, A. Fisher, R. Garcia, B. Gibson, S. Lancaster, J. Marshall and I. Whiteside, *J. Anal. At. Spectrom.*, 2015, **30**, 2249–2294.
64 J. McFarlane, S. Barth, M. Swaffer, J. E. H. Sansom and P. R. Slater, *Ionics*, 2002, **8**, 149–154.
65 D. A. Rusak, B. C. Castle, B. W. Smith and J. D. Winefordner, *Crit. Rev. Anal. Chem.*, 1997, **27**, 257–290.
66 D. W. Hahn and N. Omenetto, *Appl. Spectrosc.*, 2012, **66**, 347–419.
67 V. V. Kharton, A. L. Shaula, M. V. Patrakeev, J. C. Waerenborgh, D. P. Rojas, N. P. Vyshatko, E. V. Tsipis, A. A. Yaremchenko and F. M. B. Marques, *J. Electrochem. Soc.*, 2004, **151**, A1236.
68 J. S. Cowpe, R. D. Moorehead, D. Moser, J. S. Astin, S. Karthikeyan, S. H. Kilcoyne, G. Crofts and R. D. Pilkington, *Spectrochim. Acta, Part B*, 2011, **66**, 290–294.
69 V. N. Stathopoulos, V. C. Belessi, T. V. Bakas, S. G. Neophytides, C. N. Costa, P. J. Pomonis and A. M. Efstathiou, *Appl. Catal., B*, 2009, **93**, 1–11.
70 X. G. Cao and S. P. Jiang, *J. Mater. Chem. A*, 2014, **2**, 20739–20747.
71 E. J. Abram, D. C. Sinclair and A. R. West, *Int. J. Hydrogen Energy*, 2001, **11**, 1978–1979.